Korean J. Chem. Eng., 36(8), 1243-1248 (2019)
DOI: 10.1007/s11814-019-0309-8

pISSN: 0256-1115
eISSN: 1975-7220

Effect of precipitation on physico-chemical and catalytic properties of Cu-Zn-Al catalyst for water-gas shift reaction

Hyun-Suk Na*, Seon-Yong Ahn*, Jae-Oh Shim*, Kyung-Won Jeon*, Hak-Min Kim*, Yeol-Lim Lee*, Won-Jun Jang, Byong-Hun Jeon***,†, and Hyun-Seog Roh*,†**

*Department of Environmental Engineering, Yonsei University, 1 Yonseidae-gil, Wonju, Gangwon 26493, Korea
**Department of Environmental and Energy Engineering, Kyungnam University, 7 Kyungnamdaehak-ro, Changwon-si, Gyeongsangnam-do 51767, Korea
***Department of Earth Resources and Environmental Engineering, Hanyang University, 222 Wangsimni-ro, Seongdong-gu, Seoul 04763, Korea
(*Received 23 January 2019 • accepted 25 May 2019*)

Abstract−To investigate the effect of precipitation on physico-chemical and catalytic properties of Cu-Zn-Al catalyst, the pH value and injection rate in the precipitation process were systematically changed, and the water-gas shift reaction was carried out. The Cu-Zn-Al catalyst showed the highest CO conversion when the optimized synthesis parameters (i.e., pH=10-10.5 and injection rate=30 ml/min) were employed. This is mainly due to the enhanced physicochemical properties such as a high Brunauer-Emmett-Teller surface area, small crystallite size, high Cu dispersion, and easier reducibility.

Keywords: Water-gas Shift, Cu-Zn-Al, Precipitation Process, pH, Injection Rate

INTRODUCTION

Ternary Cu-Zn-Al catalysts have been successfully employed in important industrial processes such as the water-gas shift (WGS) reaction and methanol synthesis [1-6]. The preparation of the Cu-Zn-Al catalyst is still a subject of interest because the precursor mixture and its evolution during the preparation processes seem to affect the catalytic properties [7,8]. Several techniques for its preparation have been reported, including the impregnation method [9], sol-gel synthesis [10], hydrothermal synthesis [11], co-precipitation method [4,12,13], and microemulsion method [14]. Among these, the co-precipitation method is a commonly used method for the synthesis of nanosized materials due to several benefits: it is an environmentally benign method, it has a high reproducibility, and low cost, and it enables easy handling of the microstructure [15]. The synthesis parameters during the co-precipitation process, especially temperature, pH, and ageing time, have been considered to significantly affect the catalytic properties of the final catalyst. Furthermore, the optimal parameter values depend on the type of material [16]. Many researchers have studied a series of samples by considering a few parameters or parts of the preparation process; however, these researches concentrated on the Cu/ZnO catalyst or activities of Cu-Zn-Al catalysts in methanol synthesis reaction.

Cu-Zn-Al catalyst has been widely used for methanol synthesis, and it has been reported that various synthesis parameters affected the catalytic performance. Li et al. reported the effect of pH and temperature in the precipitation process in Cu-Zn-Al catalyst for synthesis of methanol, and concluded that both the pH value and temperature were important factors determining the interdispersion and catalytic activity for methanol synthesis [17]. Jung et al. reported that the pH changes during ageing play a significant role in the production of a high specific surface area of the Cu-Zn-Al catalyst as well as in increasing the porosity and catalytic activity in methanol synthesis [18]. Baltes et al. investigated the effect of temperature of precipitation, pH, and temperature of calcination of the Cu-Zn-Al catalyst in synthesis of methanol and found the optimum conditions for each process, such as temperature of precipitation, pH, and the temperature of calcination [19]. Bem et al. reported that the precipitation condition of the Cu-Zn catalyst, especially in pH controlling, significantly affected microstructural properties of the catalyst [20]. Simson et al. reported that control of pH value, temperature, and ageing time affected the physicochemical properties of ternary $Cu/ZnO/Al_2O_3$ catalysts for methanol synthesis [4]. Xiao et al. observed that BET surface area, Cu surface area, particle size, and interaction between Cu and ZnO of Cu-Zn-Al-Zr catalyst were affected by pH values in co-precipitation process [8]. In our previous study [21], we observed that the titration process affected significantly the properties of Cu based catalyst in the WGS reaction, and investigated the time for titration to produce highly active Cu/CeO_2 catalyst. Although many researches on synthesis parameters for preparing Cu-Zn-Al catalyst have been performed [18,19,22-25], only a few on injection rate for synthesis of Cu-Zn-Al catalyst have been reported. In addition, although the use of Cu-Zn-Al catalysts for the WGS reaction has been extensively researched, most of these studies utilized ideal reaction conditions and did not probe the effects of both pH and injection rate on catalyst performance. Therefore, it is necessary to investigate the effect of pH and injection rate for synthesis of Cu-Zn-Al and influence of

†To whom correspondence should be addressed.
E-mail: hsroh@yonsei.ac.kr, bhjeon@hanyang.ac.kr

physicochemical properties of Cu-Zn-Al in the WGS reaction.

The purpose of this research was to find and optimize the effect of the synthesis parameters (pH and injection rate in the precipitation procedure) on the catalytic properties and catalytic activity of the Cu-Zn-Al catalyst for the WGS reaction. We tried to find the effect of pH and injection rate in precipitation process for synthesis of Cu-Zn-Al catalyst; the higher injection rate resulted in the higher catalytic activity in the WGS reaction. Furthermore, pH values in precipitation process significantly affected the catalytic properties of Cu-Zn-Al catalysts. The effect of synthesis parameters was analyzed by using the Brunauer-Emmett-Teller (BET), hydrogen-temperature programmed reduction (H_2-TPR), N_2O-chemisorption, X-ray diffraction (XRD) and related to the activity tests in the WGS reaction.

EXPERIMENTAL

1. Catalyst Preparation

The Cu-Zn-Al (CZA) catalysts were produced by a co-precipitation method. The loading amounts of Cu and Zn were set at 65 wt% and 25 wt%, respectively. Following the dissolution of $Cu(NO_3)_3 \cdot xH_2O$ (99% Aldrich), $Zn(NO_3)_2 \cdot 6H_2O$ (99% Aldrich), and $Al(NO_3)_3 \cdot 9H_2O$ (99% Aldrich) in DI water, a 15 wt% potassium hydroxide solution was injected (maintaining constant stirring at 80 °C and using an injection rate of 30 ml/min) until a pH of x (x=9.5, 10, 10.5, 11) was realized. The injection rate of the 15 wt% potassium hydroxide solution was systemically changed between 0.5 and 30 ml/min, and the precipitate was stirred at 80 °C for three days. The as-obtained precipitate was washed by using DI water. After washing, the solid product was dried at 110 °C for 10 h and calcined at 400 °C for 6 h in air.

2. Characterization

The XRD measurements involved using a Rigaku D/MAX-IIIC diffractometer with nickel-filtered Cu-Kα radiation and operation at 100 mA and 40 kV. The prepared samples were scanned between 20 and 80°, with a step size of 0.02°. The crystallite size was calculated from the full width at half maximum (FWHM) of the (111) line using Debye-Scherrer equation as shown in the following equation [26],

$$D = \frac{K\lambda}{\beta \cos\theta} \quad (1)$$

where K is the constant; λ is the radiation wavelength; β is the FWHM; and θ is the peak position.

The BET surface area was calculated by measuring N_2 isotherms at 77 K using an ASAP 2010 (Micromeritics) [26]. Prior to BET analysis, catalysts were degassed for 10 h at 110 °C in a vacuum of 10^{-5} torr.

The Cu dispersion was measured by N_2O-chemisorption (Autochem 2920, Micromeritics) as earlier explained [27,28].

The hydrogen-TPR measurements were achieved by an Autochem 2920 (Micromeritics) using a previously reported method [29]. The measurement was carried out using 10% H_2 in Ar gas and a heating rate of 10 °C/min.

X-ray photoelectron spectroscopy (XPS) was carried out using a K-Alpha (Thermo-Scientific) spectrometer with an Al Kα monochromator. Before analysis, the catalysts was reduced at 400 °C for 1 h. XPS survey scans were obtained with a pass energy of 100 eV and high resolution scanning was performed at a pass energy of 50 eV [30].

3. Catalytic Reaction

The activities of the prepared catalysts were performed over a temperature range of 200 to 240 °C at 1 atm in a quartz type reactor (I.D.: 4 mm) [30,31]. 0.1 g of the samples was packed and mounted onto the layer of wool in the reactor. The quartz reactor was located in a furnace. The temperature was observed using a K-type thermocouple [32]. The composition of the reactant gas was 9 vol% CO, 10 vol% CO_2, 1 vol% CH_4, 60 vol% H_2, and 20 vol% N_2. The flow of feed gases was managed by mass flow controllers (Brooks 5850E). Before the reaction, the prepared catalyst was reduced in situ in a 2 vol% H_2/N_2 flow at 200 °C for 1 h. The feed $H_2O/(CH_4+CO+CO_2)$ ratio was fixed at 2 : 1. A gas hourly space velocity (GHSV) was 8,001-16,002 h^{-1}. The effluent gas mixture was analyzed using a micro-GC (Agilent 3000) equipped with dual channels: one with a molecular sieve and the other with Plot U and a TCD detector [33].

RESULTS AND DISCUSSION

1. Effect of pH

1-1. Catalyst Characterization

The pH is a crucial parameter that influences the properties of nanoparticles in wet chemical methods [34-36]. Following the preparation of CZA catalysts using different pH values in the precipitation process, the CZA catalysts were analyzed using various characteristics and the results are in Table 1. The BET surface area increases with pH from 9.5 to 10.5; however, a further increase in pH causes a drastic decrease in the BET surface area. Therefore, the CZA catalyst prepared with pH 10.5 exhibited the highest BET surface area value of 60.7 m^2/g. Thus, in the pH in precipitation process, the pH affects the BET surface area. According to the literature [37], pH value affected the electrostatic repulsion, which is a force to prevent aggregation. Thus, the lowest surface area of the CZA catalyst prepared at pH value of 11 may due to weak (near to 0 mV) electrostatic repulsion. It is generally known that high BET surface area can enhance activity of the catalyst by yielding a higher number of surface active sites that are accessible for adsorbing reactants.

Fig. 1 displays the XRD results of the CZA catalysts with various pH values. For all the CZA catalysts, diffraction peaks of copper

Table 1. Characteristics of CZA catalysts prepared by different pH

Catalyst	BET surface area[a] (m^2/g)	Crystallite size of CuO[b] (nm)	Cu dispersion[c] (%)
CZA (pH 9.5)	55.5	13.2	0.53
CZA (pH 10)	60.2	12.2	0.69
CZA (pH 10.5)	60.7	12.3	0.70
CZA (pH 11)	32.9	14.3	0.20

[a]Estimated from N_2 adsorption at −196 °C

[b]Calculated from XRD

[c]Estimated from N_2O chemisorption

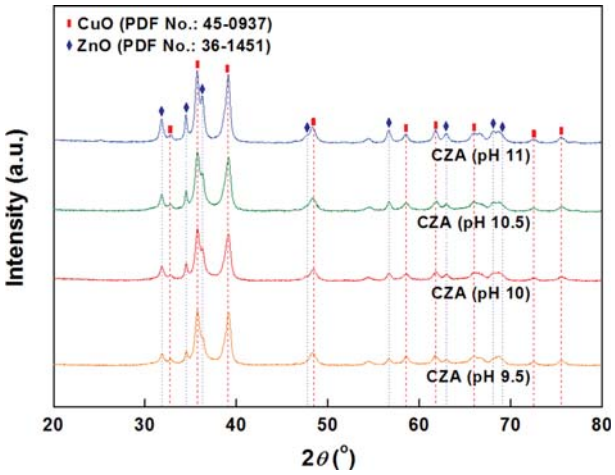

Fig. 1. XRD patterns of CZA catalysts prepared by different pH.

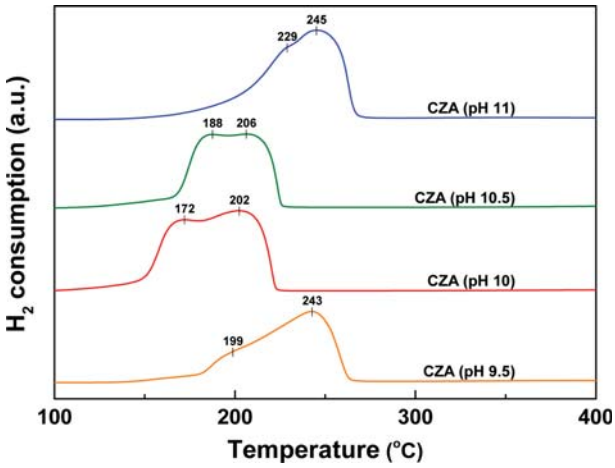

Fig. 2. TPR patterns of CZA catalysts prepared by different pH.

oxide (JCPDS 45-0937) [38] and zinc oxide (JCPDS 36-1451) [39] crystallites are observed. In contrast, the diffraction peak of Al_2O_3 is not detected in all the CZA catalysts because of its low content and peak overlapping with CuO and ZnO. XRD peak broadening differs depending on the pH value. This indicates that the crystallite size of the catalyst is strongly affected by the pH value in the precipitation process. For comparison of the crystallite size of CuO, the crystallite size from the 39.2° peak was evaluated using Debye-Scherrer equation. The CuO crystallite size varied from 12.2 to 14.3 nm. When the pH value was increased from 9.5 to 10, the crystallite size of CuO decreased from 13.2 to 12.2 nm; however, a further increase in pH resulted in an increase in the crystallite size of CuO. Further, the CZA catalyst with a pH value of 10 exhibited the smallest CuO crystallite size, while the catalyst with a pH value of 11 showed the biggest CuO crystallite size.

Table 1 also summarizes the N_2O-chemisorption results. It is found that Cu dispersion of the prepared CZA catalyst is consistent with the trend of the BET surface area. Therefore, the Cu dispersion of CZA catalyst was found to decrease in the following order: pH 10.5>pH 10>pH 9.5>pH 11. Moreover, the CZA catalyst with a pH value of 11 shows the lowest Cu dispersion (0.2%) which is about 3.5-times lower than that of CZA catalysts with a pH value of 10-10.5. This might be explained by the presence of excess KOH that adversely affects Cu dispersion. Cu dispersion is an important factor affecting the WGS reaction because higher Cu dispersion provides a greater number of active sites. This phenomenon implies that the higher Cu dispersion should be realized to enhance the catalytic activity for the WGS reaction.

H_2-TPR analysis was carried out for evaluating the reduction property of the CZA catalysts, as displayed in Fig. 2. All the prepared catalysts show two reduction peaks at around 200 °C. According to the literature [3,18], these peaks can be attributed to the stepwise reduction of $Cu^{2+} \rightarrow Cu^{1+} \rightarrow Cu^0$. Cu^0 is well known as the main active site for the WGS reaction [44]. For pH values from 9.5 to 10, reduction peaks shifted to lower temperatures with increasing pH value. However, a further increase in the pH value resulted in a shift to a higher temperature. These results therefore suggest that the CZA catalyst with a pH 10 exhibits easier reducibility than the

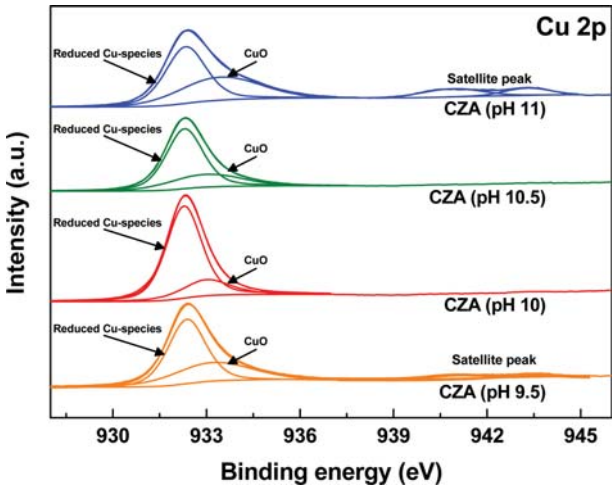

Fig. 3. XPS spectra of CZA catalysts prepared by different pH (Cu 2p).

others, and that the pH in the process of precipitation can affect not only physical properties of the catalyst but also chemical properties.

The valence states of Cu in the CZA catalyst and surface composition were investigated by XPS measurement. Fig. 3 shows the Cu 2p spectra of the CZA catalysts reduced at 200 °C for 1 h. The peak of the Cu 2p binding energy appeared at 932 eV for all the samples, all of which could be deconvoluted into two main peaks. These can be attributed to reduced copper species (Cu^{1+}, Cu^0) and copper oxide (Cu^{2+}), respectively, whereas the satellite peak at 942

Table 2. Surface atomic ratios estimated by XPS

Catalyst	Cu species (%)	
	Reduced Cu	CuO
CZA (pH 9.5)	64	36
CZA (pH 10)	80	20
CZA (pH 10.5)	74	26
CZA (pH 11)	50	50

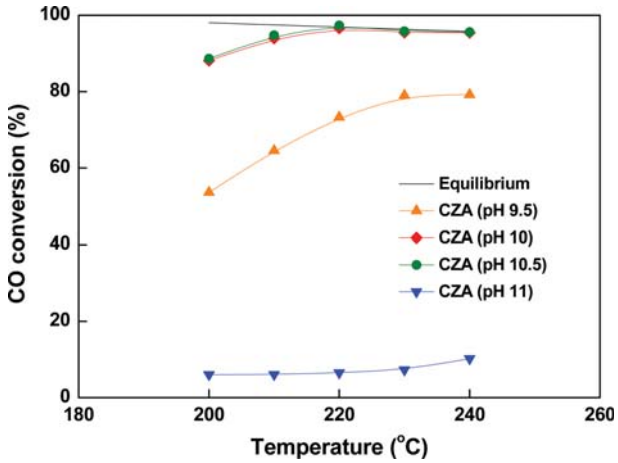

Fig. 4. CO conversion with reaction temperature over CZA catalysts prepared by different pH ($H_2O/(CH_4+CO+CO_2)$=2.0; GHSV= 8,001 h^{-1}).

eV was attributed to the Cu^{2+} species of CuO. The relative surface composition was determined from integrated peaks, and the consequences are listed in Table 2. As shown, the major component on the surface of prepared CZA catalysts was the reduced Cu species. Note that the ratio of reduced Cu species was altered with the pH value. The ratio of the reduced Cu species increased with the pH value up to 10, while it decreased when the pH value increased from 10 to 11. This result matches well with the TPR result, so it is able to be decided that the easier reducibility of the catalyst helps to maintain reduced Cu species that is the active phase in the WGS reaction [40]. Thus, it is expected that the CZA catalyst that has a higher amount of reduced Cu species shows a higher catalytic activity for the WGS reaction.

1-2. Catalytic Performance

To find the effect of pH in the precipitation process, we tested the WGS activity of CZA catalysts at the GHSV of 8,001 h^{-1}. The CO conversion over CZA catalysts is displayed in Fig. 4. The CO conversion of CZA catalysts increased with the pH from 9.5 to 10, but a further increase in the pH (over 10.5) caused a critical conversion drop in the WGS reaction. Therefore, in all the reaction temperature ranges, the CZA catalyst with a pH value of 11 exhibited the lowest CO conversion (<10%); in contrast, the CZA catalysts with pH ranging from 10 to 10.5 showed the highest CO conversion that was close to the thermodynamic equilibrium at above 220 °C.

The above-mentioned reaction results could be accounted for as follows. First, a high surface area and the small crystallite size of CZA catalysts were obtained at pH of 10-10.5, which are associated with high catalytic activity because these can help to increase the surface active sites [30,41]. Second, Cu dispersion that results in the small crystallite size and high BET surface area is promoted by using a pH of 10-10.5 in precipitation process, which has a critical effect on the catalytic activity. In addition, easier reducibility of the CZA catalyst is partly responsible for improved catalytic activity.

In this session, the optimal pH value in the precipitation process was identified by using the catalytic activity test and the reason was discussed with related characterization. In the next session, we aim to focus on the best way to obtain a pH of 10.5 in the precipitation process for the synthesis of CZA catalyst.

Table 3. Characteristics of CZA catalysts prepared by different injection rate

Catalyst	BET surface area[a] (m^2/g)	Crystallite size of CuO[b] (nm)	Cu dispersion[c] (%)
CZA (30 ml/min)	60.7	12.3	0.70
CZA (15 ml/min)	56.8	12.7	0.64
CZA (1 ml/min)	49.1	13.0	0.55
CZA (0.5 ml/min)	48.1	13.1	0.50

[a]Estimated from N_2 adsorption at −196 °C
[b]Calculated from XRD
[c]Estimated from N_2O chemisorption

2. Effect of Injection Rate

2-1. Catalyst Characterization

Titration is an important process in the co-precipitation method because the titration method critically affects catalytic properties, such as the crystallite size, BET surface area, and metal dispersion [21]. To elucidate the effect of the injection rate on the CZA catalysts for the WGS reaction, a number of characterizations were used. As listed in Table 3, a decrease in the BET surface area with decreasing injection rate is observed. This implies that the injection rate affects significantly the BET surface area, which agrees with previous study results [21].

The XRD patterns displayed in Fig. 5 reveal diffraction peaks corresponding to copper oxide (JCPDS 45-0937) [42] and zinc oxide (JCPDS 36-1451) [43] crystallites of the CZA catalysts with different injection rates. When the injection rate is decreased, the intensity of the ZnO diffraction peak is also slightly increased. In case of Al_2O_3, the diffraction peak is not found in all samples due to its low loading amount and peak overlapping. To evaluate the effect of the injection rate on the crystallite size of CuO, the size of crystallite was determined by using the Debye-Scherrer equation and summarized in Table 3. As shown, the crystallite size of CuO of the CZA catalyst increases from 12.3 to 13.1 nm with increasing the injection rate; therefore, the CZA catalyst with an injection rate of

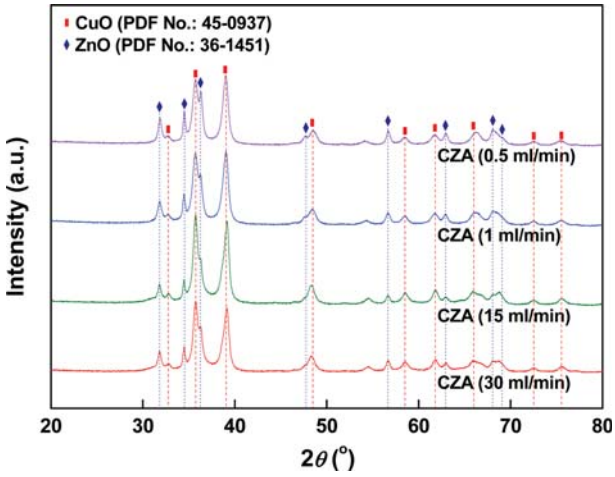

Fig. 5. XRD patterns of CZA catalysts prepared by different injection rate.

30 ml/min has the smallest crystallite size of CuO, while the CZA catalyst with an injection rate of 0.5 ml/min exhibits the biggest crystallite size of CuO.

The Cu dispersions of the CZA catalysts are exhibited in Table 3. As indicated, an increase in the injection rate caused an increase in the Cu dispersion. Note that the Cu dispersion result of the CZA catalysts shows a trend similar to that of the BET results.

Hydrogen-TPR was carried out to analyze the characteristics of reduction of the CZA catalysts, as displayed in Fig. 6. All CZA catalysts exhibit two reduction peaks at around 200 °C caused by the stepwise reduction of $Cu^{2+} \rightarrow Cu^{1+} \rightarrow Cu^{0}$ [3,18]. Reduction peaks of CZA catalysts with different injection rates are shifted to a higher temperature with decreasing injection rate. This implies that CZA catalyst with an injection rate of 30 ml/min exhibits easier reducibility than the others.

2-2. Catalytic Performance

To elucidate the relationship between the injection rate and the activity of the catalyst, the WGS reaction data obtained from the CZA catalysts prepared with different injection rates are shown in Fig. 7. When the injection rate was increased, the CO conversion of the CZA catalyst was also increased. As a result, the injection rate of the CZA catalyst significantly affected the CO conversion of CZA catalysts.

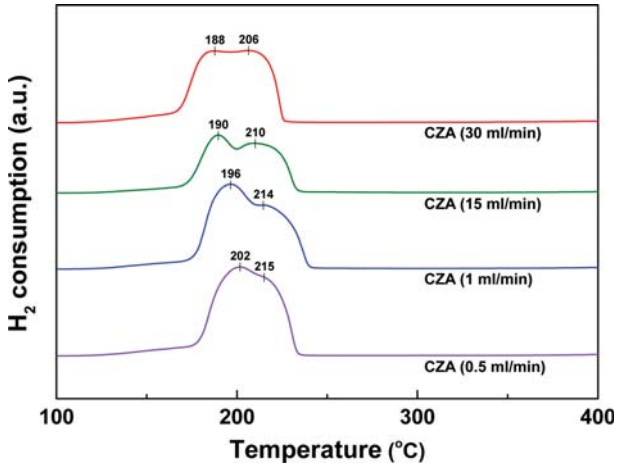

Fig. 6. TPR patterns of CZA catalysts prepared by different injection rate.

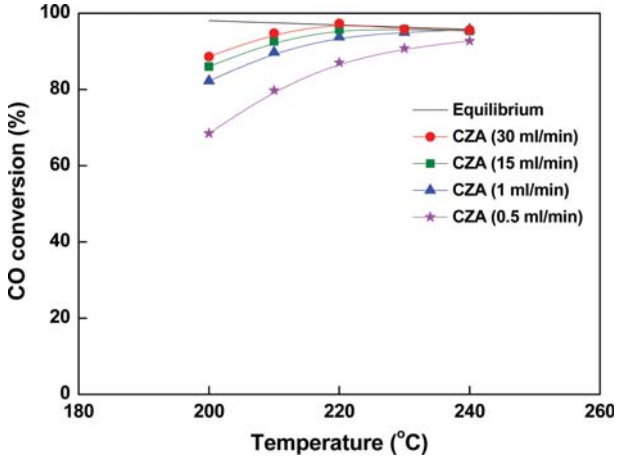

Fig. 7. CO conversion with reaction temperature over CZA catalysts prepared by different injection rate ($H_2O/(CH_4+CO+CO_2)$= 2.0; GHSV=8,001 h^{-1}).

The high catalytic activity of the CZA catalyst with a high injection rate is due to its large surface area, high dispersion of copper, and small crystallite size. With a higher injection rate, a larger surface area, higher dispersion of copper, and smaller size of crystallite are obtained. This can be explained through the crystallization of the CZA catalyst. When crystallization occurs in the precipitation procedure, the higher injection rate causes higher amounts of local supersaturation, which increases the chance of nucleation and decreases size of crystallite because the nucleation is more advantageous than crystal growth in the supersaturation condition [21, 44,45]. In addition, the larger BET surface area and smaller size of crystallite cause promoted dispersion of copper on the CZA catalysts, which provides further active sites for the WGS reaction. Furthermore, the injection rate also affects the reducibility of CZA catalysts. Enhanced reducibility of the CZA catalyst obtained with an injection rate of 30 ml/min enhances the catalytic activity for the WGS reaction [46].

To evaluate the stability of the CZA catalyst, the GHSV was doubled to 16,002 h^{-1} and the WGS reaction was performed at 240 °C for 200 h. Fig. 8 exhibits the stability test results of the optimized CZA catalyst (pH=10 and injection rate=30 ml/min). In spite of the higher GHSV, the optimized CZA catalyst showed stable CO conversion that was close to the thermodynamic equilibrium at 240 °C during 200 h. As a result, it can be concluded that the optimized CZA catalyst possessed excellent catalytic stability as well as the highest catalytic activity.

CONCLUSIONS

We determined the effect of pH and injection rate in the precipitation process and optimized them for CZA catalysts for the WGS reaction. Controlling the pH and injection rate was anticipated to have a critical effect on the physicochemical properties of CZA catalysts: we optimized the pH and injection rate to enhance

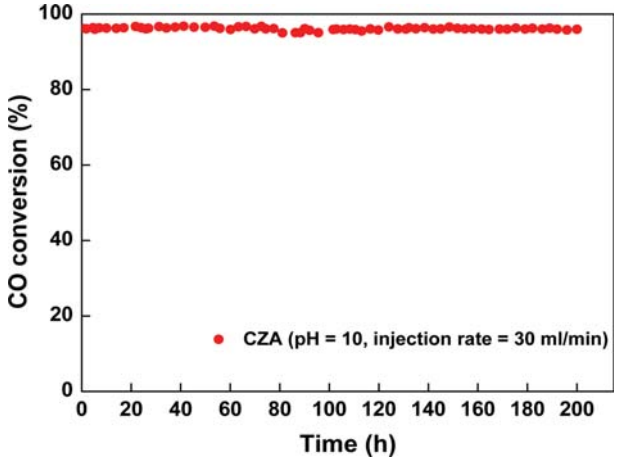

Fig. 8. CO conversion with time on stream over CZA catalyst ($H_2O/(CH_4+CO+CO_2)$=2.0; GHSV=16,002 h^{-1}; T=240 °C).

the catalytic activity for the WGS reaction. Among the prepared catalysts, the CZA catalyst with a pH value of 10-10.5 and injection rate of 30 ml/min showed the highest CO conversion. The remarkable catalytic activity of the CZA catalyst was mainly dependent on the high Cu dispersion resulting from a high surface area and small size of crystallite and partly on the easier reducibility.

ACKNOWLEDGEMENTS

This work was conducted under the framework of the research and development program of the Korea Institute of Energy Research (B7-2424). It was supported (in part) by the Yonsei University Research Fund of 2019.

REFERENCES

1. K. Nishida, I. Atake, D. Li, T. Shishido, Y. Oumi, T. Sano and K. Takehira, *Appl. Catal. A-Gen.*, **337**, 48 (2008).
2. T. Shishido, M. Yamamoto, D. Li, Y. Tian, H. Morioka, M. Honda, T. Sano and K. Takehira, *Appl. Catal. A-Gen.*, **303**, 62 (2006).
3. W. Fu, Z. Bao, W. Ding, K. Chou and Q. Li, *Catal. Commun.*, **12**, 505 (2011).
4. G. Simson, E. Prasetyo, S. Reiner and O. Hinrichsen, *Appl. Catal. A-Gen.*, **450**, 1 (2013).
5. P. Kowalik, W. Próchniak, M. Konkol and T. Borowiecki, *Appl. Catal. A-Gen.*, **423-424**, 15 (2012).
6. P. Kowalik, W. Próchniak and T. Borowiecki, *Catal. Today*, **176**, 144 (2011).
7. A. Lima, M. Nele, E. Moreno and H. M. C. Andrade, *Appl. Catal. A-Gen.*, **171**, 31 (1998).
8. S. Xiao, Y. Zhang, P. Gao, L. Zhong, X. Li, Z. Zhang, H. Wang, W. Wei and Y. Sun, *Catal. Today*, **281**, 327 (2017).
9. J.-P. Shen and C. Song, *Catal. Today*, **77**, 89 (2002).
10. Y. Guo, W. Meyer-Zaika, M. Muhler, S. Vukojević and M. Epple, *Eur. J. Inorg. Chem.*, **2006**, 4774 (2006).
11. S. Saedy, M. Haghighi and M. Amirkhosrow, *Particuology*, **10**, 729 (2012).
12. M. Behrens, D. Brennecke, F. Girgsdies, S. Kißner, A. Trunschke, N. Nasrudin, S. Zakaria, N. F. Idris, S. B. A. Hamid, B. Kniep, R. Fischer, W. Busser, M. Muhler and R. Schlögl, *Appl. Catal. A-Gen.*, **392**, 93 (2011).
13. A. Budiman, M. Ridwan, S. M. Kim, J.-W. Choi, C. W. Yoon, J.-M. Ha, D. J. Suh and Y.-W. Suh, *Appl. Catal. A-Gen.*, **462-463**, 220 (2013).
14. S. Kühl, M. Friedrich, M. Armbrüster and M. Behrens, *J. Mater. Chem.*, **22**, 9632 (2012).
15. J. Thomas, N. Thomas, F. Girgsdies, M. Beherns, X. Huang, V. D. Sudheesh and V. Sebastian, *New J. Chem.*, **41**, 7356 (2017).
16. W.-J. Jang, H.-M. Kim, J.-O. Shim, S.-Y. Yoo, K.-W. Jeon, H.-S. Na, Y.-L. Lee, D.-W. Jeong, J. W. Bae and I. W. Nah, *Green Chem.*, **20**, 1621 (2018).
17. J.-L. Li and T. Inui, *Appl. Catal. A-Gen.*, **137**, 105 (1996).
18. H. Jung, D.-R. Yang, O.-S. Joo and K.-D. Jung, *Bull Korean Chem. Soc.*, **31**, 1241 (2010).
19. C. Baltes, S. Vukojevic and F. Schuth, *J. Catal.*, **258**, 334 (2008).
20. B. Bems, M. Schur, A. Dassenoy, H. Junkes, D. Herein and R. Schlögl, *Chem. Eur. J.*, **9**, 2039 (2003).
21. H.-S. Na, J.-O. Shim, W.-J. Jang, K.-W. Jeon, H.-M. Kim, Y.-L. Lee, D.-W. Lee, S.-Y. Yoo, J. W. Bae, C. V. Rode and H.-S. Roh, *Catal. Today*, **309**, 83 (2018).
22. S. Allahyari, M. Haghighi, A. Ebadi and H. Q. Saeedi, *J. Power Sources*, **272**, 929 (2014).
23. H. Ajamein and M. Haghighi, *Ceram. Int.*, **42**, 17978 (2016).
24. H. Ajamein, M. Haghighi and S. Alaei, *Mater. Res. Bull*, **102**, 142 (2018).
25. S. Allahyari, M. Haghighi, A. Ebadi and S. Hosseinzadeh, *Energy Convers. Manage.*, **83**, 212 (2014).
26. H.-S. Na, C.-I. Ahn, A. Jha, K. S. Park, W.-J. Jang, J.-O. Shim, D.-W. Jeong, H.-S. Roh and J. W. Bae, *RSC Adv.*, **6**, 52754 (2016).
27. D.-W. Jeong, H.-S. Na, J.-O. Shim, W.-J. Jang, H.-S. Roh, U. H. Jung and W. L. Yoon, *Int. J. Hydrogen Energy*, **39**, 9135 (2014).
28. D.-W. Jeong, W.-J. Jang, J.-O. Shim, W.-B. Han, H.-S. Roh, U. H. Jung and W. L. Yoon, *Renew. Energy*, **65**, 102 (2014).
29. H.-S. Na, J.-O. Shim, S.-Y. Ahn, W.-J. Jang, K.-W. Jeon, H.-M. Kim, Y.-L. Lee, K.-J. Kim and H.-S. Roh, *Int. J. Hydrogen Energy*, **43**, 17718 (2018).
30. H.-S. Na, D.-W. Jeong, W.-J. Jang, J.-O. Shim and H.-S. Roh, *Int. J. Hydrogen Energy*, **40**, 12268 (2015).
31. J. O. Shim, Y. J. Hong, H. S. Na, W. J. Jang, Y. C. Kang and H. S. Roh, *ACS Appl. Mater. Interfaces*, **8**, 17239 (2016).
32. K.-W. Jeon, J.-O. Shim, W.-J. Jang, D.-W. Lee, H.-S. Na, H.-M. Kim, Y.-L. Lee, S.-Y. Yoo, H.-S. Roh and B.-H. Jeon, *Renew. Energy*, **131**, 144 (2019).
33. Y.-L. Lee, A. Jha, W.-J. Jang, J.-O. Shim, K.-W. Jeon, H.-S. Na, H.-M. Kim, D.-W. Lee, S.-Y. Yoo, B.-H. Jeon, J. W. Bae and H.-S. Roh, *Top Catal.*, **60**, 721 (2017).
34. A. Amirsalari and S. F. Shayesteh, *Superlattices Microstruct.*, **82**, 507 (2015).
35. G. Amin, M. Asif, A. Zainelabdin, S. Zaman, O. Nur and M. Willander, *J. Nanomaterials*, **2011**, 1 (2011).
36. Y. Y. Chu, Z. B. Wang, Z. Z. Jiang, D. M. Gu and G. P. Yin, *Fuel Cells*, **10**, 914 (2010).
37. Q. Wang, M. Cui, Y. Hou, Q. Zhong, M. Yue and X. Huang, *J. Alloys Compd.*, **712**, 431 (2017).
38. Y. Sun, L. Ma, B. Zhou and P. Gao, *Int. J. Hydrogen Energy*, **37**, 2336 (2012).
39. P. Guo, L. Chen, Q. Yang, M. Qiao, H. Li, H. Li, H. Xu and K. Fan, *Int. J. Hydrogen Energy*, **34**, 2361 (2009).
40. S. Y. Yao, W. Q. Xu, A. C. Johnston-Peck, F. Z. Zhao, Z. Y. Liu, S. Luo, S. D. Senanayake, A. Martinez-Arias, W. J. Liu and J. A. Rodriguez, *Phys. Chem. Chem. Phys.*, **16**, 17183 (2014).
41. D.-W. Jeong, W.-J. Jang, J.-O. Shim, W.-B. Han, K.-W. Jeon, Y.-C. Seo, H.-S. Roh, J. H. Gu and Y. T. Lim, *J. Mater. Cycles Waste Manage.*, **16**, 650 (2014).
42. J. A. Gomez-Cuaspud and M. Schmal, *Int. J. Hydrogen Energy*, **38**, 7458 (2013).
43. X. Yang, W. Wang, J. Xiong, L. Chen and Y. Ma, *Int. J. Hydrogen Energy*, **40**, 12604 (2015).
44. Y. Wang, Z. Li and G. P. Demopoulos, *J. Cryst. Growth*, **310**, 1220 (2008).
45. E. Kramer, J. Podurgiel and M. Wei, *Mater. Lett.*, **131**, 145 (2014).
46. H. Yahiro, K. Murawaki, K. Saiki, T. Yamamoto and H. Yamaura, *Catal. Today*, **126**, 436 (2007).